Journal Name

ARTICLE TYPE

Cite this: DOI: 10.1039/xxxxxxxxxx

High-resolution electron-induced Ge L X-ray spectrum: diagram lines and satellite structures

Andrés Sepúlveda,*[a] Tabatha Rodríguez,[a] Alejo Carreras,[b] Gustavo Castellano,[b] and Jorge Trincavelli[b]

Received Date
Accepted Date

DOI: 10.1039/xxxxxxxxxx

www.rsc.org/journalname

The L X-ray spectrum induced by electron impact upon a solid germanium target was measured with high spectral resolution and analyzed using the POEMA fitting software. Characteristic transition energies, natural linewidths, and relative radiative transition probabilities were determined for the main diagram lines. In addition, a comprehensive identification of satellite decays was achieved, including features previously unreported; the corresponding energy shifts were found to agree with literature values. New satellite structures in the Lℓ and Lη regions were also observed, the large linewidths found suggesting contributions from multiple unresolved transitions. The intensity-ratio analysis reveals a significant role of multivacancy states, with the Lβ_1 transition exhibiting an unusually high satellite-to-main ratio close to unity, evidenced by the careful spectral treatment carried out. To accurately reproduce this region, we applied the absorbed Voigt profile previously developed for L-emission spectra, which incorporates an energy-dependent absorption term to account for the variation of the absorption coefficient across the neighbouring L_3 edge. This approach successfully reproduces the low-energy asymmetry of the Lβ_1 peak and its effect on the relative intensities of the main and satellite components. The results obtained aim to complete the database available at present for Ge L X-ray parameters, providing methodological advances applicable to the spectroscopic study of other elements.

1 Introduction

X-ray spectra generated by electron impact can be helpful in the characterization of chemical elements. The analysis of these spectra provides information about atomic parameters associated with characteristic lines, such as transition energies, natural linewidths, and relative radiative transition probabilities (RTPs), which are fundamental not only for the development of several spectroscopic techniques, but also for validating theoretical models in atomic physics.

From a spectroscopic perspective, X-ray transitions offer valuable information about the internal electronic configuration of atoms. Early studies, such as the work published by Bearden[1], provided a comprehensive compilation of characteristic energies based on available experimental data. Subsequently, Cauchois and Sénémaud[2] determined diagram and non-diagram transition energies from Li to Am. More recently, Deslattes *et al.*[3] incorporated modern theoretical models and relativistic corrections for the assessment of transition energies. All these works furnish the basis to identify characteristic lines in X-ray spectral analyses.

In addition, several theoretical and experimental studies have addressed the determination of transition rates and natural linewidths. Scofield[4] carried out relativistic Hartree-Fock calculations, widely used as a theoretical reference due to their high accuracy, whereas Perkins *et al.*[5] provided theoretical values derived from the Evaluated Atomic Data Library (EADL). Regarding natural linewidths, Campbell and Papp[6] compiled experimental values from several decades of measurements, whereas Perkins *et al.*[5] also reported theoretical estimates for these parameters.

A typical X-ray spectrum presents not only the main diagram lines but also satellite structures appearing in the vicinity of the primary peaks. These satellites result from more complex atomic interactions and provide information about electron correlation effects, and excitation-relaxation dynamics. These features have previously been observed under different excitation conditions, including X-ray fluorescence[7,8], electron impact[9], and ion beam excitation with ^{4}He[10]. It is well established[11] that the satellite line energies are characteristic of the emitting atom and remain largely independent of the excitation mechanism, while their relative intensities depend on the nature and energy of the incident particle.

Some of the satellite structures can be attributed to radiative transitions in atoms with more than one vacancy. For example,

[a] *Facultad de Ciencias Naturales, Matemática y del Medio Ambiente, Universidad Tecnológica Metropolitana (UTEM), Chile. E-mail: andres.sepulveda@utem.cl*
[b] *Instituto de Física Enrique Gaviola (IFEG-CONICET), Facultad de Matemática, Astronomía, Física y Computación, Universidad Nacional de Córdoba, Argentina*

in the case of L X-ray emission, the presence of an additional $3d$ vacancy alters the initial state of the transition, producing a slight energy shift towards values higher than that of the corresponding diagram line. These multiple-vacancy configurations may arise through different physical processes. One possibility is direct multiple ionization, whose probability decreases rapidly with the number of electrons removed. However, for electron incidence, Coster-Kronig (CK) transitions and shake (SH) effects are more efficient mechanisms. In the case of CK transitions, the rearrangement of a vacancy between sublevels in a particular atomic shell is accompanied by the emission of an Auger electron from a more external shell. For the shake effect instead, the sudden modification of the atomic potential originated by an ionization causes the ejection of an outer electron.

Since the occurrence of spectator holes at inner atomic levels modifies the electron screening of the nuclear potential, distorting the energy levels of the atom, the presence of many bound levels in the atom favors the emission of satellite lines. In the intermediate atomic number region, germanium is a semiconductor with a broad range of technological applications, which may be useful to analyze the L-emission spectrum and study the excitation-relaxation mechanisms mentioned above. This element has historically played a central role in the fabrication of electronic devices such as X-ray detectors, transistors and diodes[12]. More recently, its optical and electronic characteristics have been exploited in infrared sensors, optical fibers, and high-efficiency solar cells, especially in space applications[13,14].

Several authors have studied the Ge-L X-ray emission spectrum by different excitation sources, like electrons[9,15], ions[10], X-ray tube photons[2,7,16], and selective excitation by synchrotron radiation[17]. Attention has been focused on the characterization of diagram linewidths[16,17] and also on the mechanisms originating satellite emissions[9,10,15–17]. In this work, the Ge L X-ray spectrum induced by electrons is analyzed in detail. Characteristic energies, relative radiative transition probabilities, and natural linewidths for the diagram lines are obtained and compared with values reported in the literature. In addition, satellite lines are identified according to their energy shifts from the associated diagram lines, enabling an interpretation of their origin. Relative intensities and peak widths of these satellite structures are also evaluated.

2 Experimental

The measurements were performed using the experimental setup described in[18]. The spectrum was acquired using an INCA Wave 700 wavelength-dispersive spectrometer (WDS), coupled to a commercial Leo 1450VP scanning electron microscope. This system operates under a Johansson type arrangement, which allows to maintain a constant take-off angle at normal electron beam incidence[19]. A thallium acid phthalate (TAP) analyzer crystal with an interplanar spacing $2d = 25.9$ Å, was selected to cover all Ge-L characteristic energies. During the experiment, the thermal conditions in the laboratory were kept stable to minimize fluctuations and ensure accurate energy calibration.

The analyzed sample consisted of a pure germanium standard (purity $> 99.9999\%$), which was polished and coated with a thin carbon layer to prevent charge accumulation and thermal damage during data acquisition. The measurements were carried out using a 20 kV acceleration voltage and a take-off angle of 29°, with an average beam current of 140.12 nA, as measured by a Faraday cup, and a total acquisition time of 104 minutes. To cover the relevant Ge-L transitions, the photon energies were scanned in the range comprised from 0.95 to 1.38 keV. Regarding the absolute detection efficiency of the system, it was characterized in a previous work[20], which involves comparing spectra obtained using both an energy-dispersive spectrometer and the WDS involved. The efficiency curve used for the TAP crystal spans the energy range from 0.521 to 1.675 keV, incorporating corrections for geometrical factors, crystal reflectivity, and the proportional counter quantum efficiency. The counting system consists of two complementary detectors operating in tandem: a P10 (90% Ar and 10% CH_4) flow proportional counter and a sealed xenon detector.

3 Spectral analysis

The analysis of the Ge L X-ray spectrum was performed over the entire measured energy range using the software POEMA[21], which has been designed to optimize atomic and experimental parameters through an iterative fitting process. The procedure consists of minimizing the χ^2 function for the set of experimental intensities I_i constituting an N-channel spectrum, defined as

$$\chi^2 = \frac{1}{N-P}\sum_i \frac{(\bar{I}_i - I_i)^2}{\bar{I}_i}, \tag{1}$$

where P is the number of refined parameters and $\bar{I}_i$ is the analytic function proposed to describe the i-th channel intensity. This model includes characteristic lines, satellite structures, bremsstrahlung radiation, and spurious peaks[21–23], corrected by the detection efficiency mentioned in the previous section. The peak widths were described considering the natural contribution associated to each transition and the instrumental broadening given by a function of the photon energy, characterized by the effective angular width of the detection system. An initial estimate for the latter was used as a starting point, and during the fitting process it was refined as a global parameter, along with the natural widths of all the transitions involved.

To achieve an accurate spectral description, three types of analytical profiles were employed, selected according to the physical characteristics of each transition. Standard Voigt profiles were used to describe the main diagram lines, whereas Gaussian profiles were applied to the satellite lines. In these cases, absorption was included as a uniform correction factor applied to the total intensity of each peak. In the particular case of the $L\beta_1$ line and its associated satellites, an absorbed Voigt profile was applied, obtained by convolving the Voigt function with an energy-dependent absorption term,

$$S_q(E) = \int L_q(E')A(E')G(E-E')\,dE', \tag{2}$$

where $A(E')$ varies sharply across the neighbouring L_3 absorption edge of the same element. This formulation accurately models the asymmetric distortion observed in the $L\beta_1$ region, where the attenuation originates not from the emitting subshell (L_2) but from a different one (L_3).

The software POEMA involves the mass attenuation coefficients given by Heinrich[24] for the estimation of the combined atomic number and absorption corrections. These matrix effects are computed on the basis of the $\phi(\rho z)$ ionization distribution model developed by Packwood and Brown[25] and improved by Riveros and Castellano[26], whereas the characteristic fluorescence enhancement is assessed according to the traditional Reed's model[27].

The inclusion of the absorbed Voigt profile follows the approach previously applied to Fe and Ni L spectra, where the absorption asymmetry originated in the same subshell[28], and here it is extended to a distinct case of cross-edge differential absorption. This correction was essential to reproduce the asymmetric shape of the Ge Lβ_1 line and to obtain physically consistent satellite-to-main intensity ratios.

The spectrometer calibration was carried out assuming a linear relationship between wavelength and channel number, governed by the *gain* and *offset* parameters. During the optimization process, the latter was refined while keeping constant the characteristic L$\alpha_{1,2}$ energy, taken from Bearden[1], as well as the *gain* value reported by the acquisition system, which is based on the crystal interplanar spacing.

As a starting point for the fitting process, the emission energies were taken from Bearden[1] for the main lines, and from Cauchois and Sénémaud[2] for the satellite lines. The initial values for the natural linewidths were taken from Campbell and Papp[6], whereas the initial relative radiative transition probabilities were assessed from the transition rates reported by Scofield[4], normalized with respect to the main lines.

The fitting procedure was initiated by considering only the diagram lines. In a first stage, global scale factors, defined independently for each emitting subshell (L_1, L_2, and L_3), were refined together with the background parameter and the energy calibration offset. The analysis of the residuals obtained from this initial fit revealed the need to include additional satellite contributions. Satellite lines previously reported in the literature were incorporated first. In cases where no prior information was available, the inspection of the residuals allowed for an initial estimation of the energies and intensities of these structures.

The presence of at least one satellite peak was noticed for each diagram line, except for the weak L$\beta_{3,4}$ transition. Each satellite line was assigned to the nearest low-energy diagram transition, using spectral proximity as the sole criterion. For the satellite linewidths, the same initial value as that of the associated diagram line was adopted. Once the satellite lines were included, the relative radiative transition probabilities were refined, followed by the simultaneous adjustment of the energies and linewidths of all the transitions considered.

Throughout the minimization process, the quality of the fit was systematically evaluated using the χ^2 value. In cases where the optimization converged to a local minimum, the line energies were manually displaced toward spectrally plausible positions and temporarily fixed, allowing the refinement of linewidths and relative transition probabilities to continue. After releasing all parameters again, a further decrease in χ^2 was achieved, leading to solutions with an improved global agreement between the model and the experimental data. Comparisons between solutions obtained from different sets of initial values confirmed that the χ^2 criterion provides a robust tool to assess the quality of the fit and to discriminate among different local minima.

The uncertainties associated with the refined parameters were evaluated following the procedure described by Bonetto *et al.*[29]. This approach consists of propagating the statistics of the experimental counts into the uncertainties of the refined parameters.

4 Results and discussion

Figure 1 shows the experimental Ge L X-ray spectrum along with the fit obtained using the software POEMA. The resulting χ^2 value of 1.09 indicates an excellent agreement between the analytic spectrum and the measured data, even in low-intensity regions. The main L-group transitions, namely Lℓ, Lη, L$\alpha_{1,2}$, Lβ_1, and L$\beta_{3,4}$, are clearly resolved. In addition, secondary features appear near the main peaks, particularly on the high-energy side of L$\alpha_{1,2}$ and Lβ_1. These partially overlapped structures have been identified as satellite transitions, as explained in the previous section. The residuals, shown as a red line, remain consistently small and free of systematic oscillations, supporting the reliability of the fit. Insets provide enlarged views of the Lℓ, Lη, and L$\beta_{3,4}$ weak transitions.

Figure 2 compares the Ge Lβ_1 spectral region fitted with (a) standard Voigt profiles and (b) the model including the energy-dependent absorption correction. When identical atomic parameters are used for the characteristic line and its satellites, the absorbed Voigt profile provides a markedly better reproduction of the experimental spectrum, particularly the asymmetry observed on the low-energy side. This behaviour reflects the influence of the neighbouring L_3 absorption edge, which differentially attenuates the emission across the line profile. At energies well above the edge, both models reproduce the spectrum with the same accuracy, as expected. This effect constitutes a clear manifestation of cross-edge differential absorption, in which the emission from the L_2 subshell is modified by the neighbouring L_3 edge of the same element. If the differential absorption were neglected, a satisfactory fit could only be achieved by artificially broadening the main line, leading to a lower satellite-to-main intensity ratio. Including this effect in the model therefore yields a more realistic description of the experimental shape and ensures a consistent determination of both the characteristic energies and the relative line intensities.

4.1 Diagram lines

Table 1 displays the characteristic energies obtained in this work, along with the reference values reported by Bearden[1], Cauchois and Sénémaud[2], and Deslattes *et al.*[3]. In the cases of the L$\alpha_{1,2}$ and L$\beta_{3,4}$ transitions, the experimental resolution did not allow for a clear separation of the doublet components. Therefore, in each case a single line representing both contributions was fitted. For comparison with literature data, weighted averages of the corresponding characteristic energies were assessed according to the emission rates reported by Scofield[4]. Since the calibration was performed relying on the L$\alpha_{1,2}$ energy reported by Bearden[1], the uncertainties displayed in this table were assessed as the quadra-

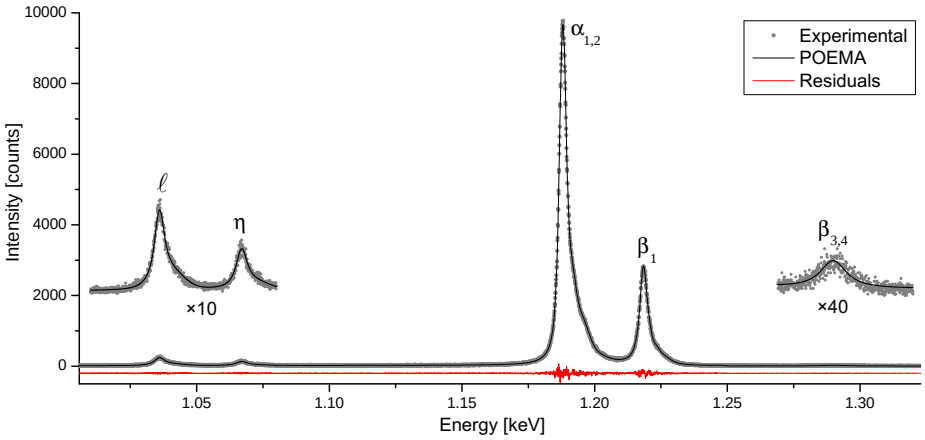

Fig. 1 Ge L X-ray spectrum. Experimental data are shown as dots, the model fit obtained using POEMA as a solid line, and the fitting residual as a red line. Insets provide magnified views of the regions corresponding to the less intense transitions.

Table 1 Characteristic energies (in keV) obtained in this work along with data previously published. The values in parentheses indicate estimated uncertainties in the last digit

Transition	This work	Ref. [1]	Ref. [2]	Ref. [3]
L_3M_1 (ℓ)	1.0360(1)	1.0362	1.0378	1.0373
L_2M_1 (η)	1.0670(1)	1.0680	1.0680	1.0683
L_2M_4 (β_1)	1.2183(1)	1.2185	1.2186	1.2189
L_1M_{23} ($\beta_{3,4}$)	1.2899(2)	1.2913	1.2913	1.2903

Table 2 Relative radiative transition probabilities obtained in this work along with data previously published. Numbers in parentheses indicate the estimated uncertainties in the last digit

Transition	This work	Ref. [4]	Ref. [5]
L_3M_1 (ℓ)	0.048(2)	0.0439	0.3128
$L_3M_{4,5}$ ($\alpha_{1,2}$)	0.95(2)	0.9519	0.6763
L_2M_1 (η)	0.028(2)	0.0403	0.3074
L_2M_4 (β_1)	0.97(12)	0.9557	0.6806

ture addition of the error estimated by the POEMA routine and the probable error provided in the original work[1]. A good general agreement is observed between the present results and the other sources quoted. Particularly, the energy shifts from Bearden's values are always below 1.5 eV, a discrepancy similar to that observed among the other authors considered.

Relative radiative transition probabilities (RTPs) obtained in this work, which include the integrated contribution of the corresponding satellite components, are presented in Table 2 together with theoretical data available in the literature. The comparison exhibits a very good agreement with Scofield[4]. In contrast, significant discrepancies are observed with the values reported by Perkins *et al.*[5]. It must be emphasized that all the data available in the literature correspond to theoretical calculations, whereas the present results are the first experimental RTP data reported for the germanium L shell.

The optimization procedure carried out has also permitted to

Table 3 Natural linewidths (in eV) obtained in this work along with data previously published. Numbers in parentheses indicate the estimated uncertainties in the last digit

Transition	This work	Ref. [5]	Ref. [6]
L_3M_1 (ℓ)	3.9(6)	4.97	2.96
L_3M_4 (α_1)	1.90(2)	0.89	0.91
L_3M_5 (α_2)		0.88	0.90
L_2M_1 (η)	4.6(1)	4.98	2.96
L_2M_4 (β_1)	0.71(3)	0.89	0.91
L_1M_2 (β_3)	11.5(4)	12.70	6.1
L_1M_3 (β_4)		12.43	6.1

determine the natural linewidths corresponding to the transitions considered. Table 3 displays the values obtained in this work, compared with two databases available in the literature[5,6]. A good overall agreement can be observed, although certain discrepancies arise between the two databases considered. For the Lℓ and Lη transitions, the linewidths obtained here lie between those reported by Perkins *et al.*[5] and by Campbell and Papp[6]. In the case of the L$\alpha_{1,2}$ doublet, the width obtained is significantly greater than the individual values found in the literature for the Lα_1 and Lα_2 transitions; nevertheless, it must be borne in mind that the comparison between the width of two separate lines and a doublet cannot be done straightforwardly. Particularly, the present linewidth is similar to the 1.8 eV reported by Leiro[16]—obtained without removing the instrumental broadening. Instead, the natural linewidth of (0.86± 0.06) eV obtained by Guerra *et al.*[17] is closer to the other data shown in Table 3. For the Lβ_1 transition, the resulting linewidth was slightly lower than the values reported by both Perkins *et al.* and Campbell and Papp, which can be attributed to the treatment of the neighbouring L_3 absorption edge in the present model. Regarding the weak L$\beta_{3,4}$ doublet, the obtained width is similar to the corresponding to each individual component reported in Ref.[5], and to the sum of the two separate components reported by Ref.[6]; the present

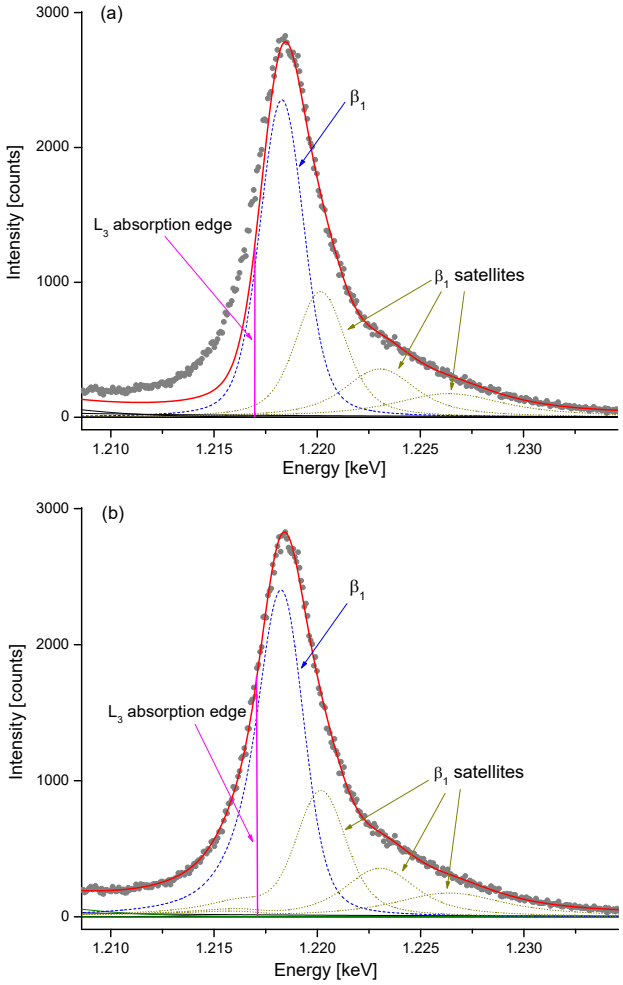

Fig. 2 Comparison between (a) the standard Voigt fit and (b) the model including the cross-edge differential absorption for the Ge Lβ_1 region. The attenuation produced by the neighbouring L_3 edge leads to an asymmetric distortion of the low-energy side of the line, which is accurately reproduced only when the energy-dependent absorption term is included in the convolution.

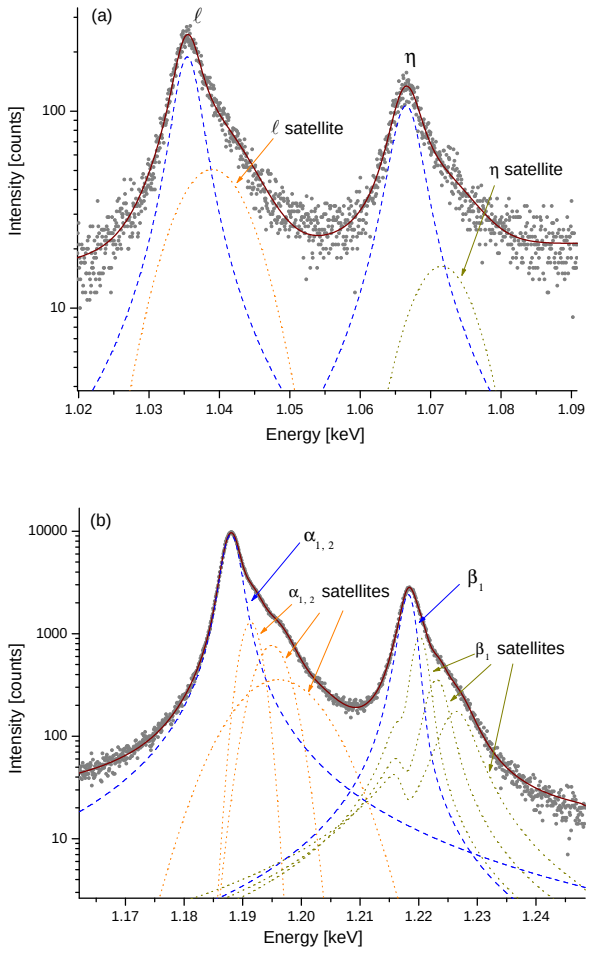

Fig. 3 Ge-L X-ray spectrum in the regions: (a) Lℓ and Lη; (b) L$\alpha_{1,2}$ and Lβ_1. The experimental data (dots), the fit obtained with POEMA (solid line), the characteristic emissions (dashed lines), and the satellite bands (dotted lines) are shown.

result suggests that the latter alternative is more adequate, bearing in mind the 8 eV energy difference between these two decays, according to Bearden.

It is worth emphasizing that the natural widths determined are significantly narrower than the peak widths involved. For example, in the case of L$\alpha_{1,2}$ a natural linewidth of (1.90 $\pm$ 0.02) eV was obtained from an experimental peak width of around 3.4 eV, which highlights the robustness of the optimization software used.

4.2 Satellite Lines

Figure 3 shows the regions of the Ge X-ray spectrum where satellite structures were identified: one corresponding to the Lη and Lℓ transitions, and the other one encompassing the L$\alpha_{1,2}$ and Lβ_1 lines. Each plot exhibits the characteristic lines together with their associated satellite structures and the spectral fit obtained using the software POEMA. All experimental energy shifts for the satellite lines determined in this work, along with the comparison with values reported in the literature, are summarized in Table 4. This table includes satellite lines documented here for the first time as well as those previously reported, the latter exhibiting a general agreement.

Different theoretical and experimental studies have attempted to identify and analyze these satellite structures, often associating them with multiple ionization states. The mechanisms leading to the formation of multivacancy configurations ($2p$,$3d$) include multiple direct ionization, Coster-Kronig transitions, and shake effects. In particular, the probability f_{12}, which describes the $L_1 \rightarrow L_2$ transition accompanied by the emission of an electron from an outer shell (such as $3d$), is relatively high for Ge ($f_{12} \approx 0.199$ according to Campbell[30]), implying this mechanism bears a prominent role in the generation of these lines. Both Lα and Lβ high energy satellite emissions were experimentally observed by Deslattes[15] and described with more detail by Leiro[16], who determined two α and one β satellites. For the case of Lα satellites, Blokhin *et al.*[9], relying on multiplet theory calculations, determined the energies and relative intensities for transitions

Table 4 Satellite lines observed and comparison of their energy shifts (ΔE in eV) with values reported in the literature

Main line	Satellite	Origin	This work	Ref. [9]	Ref. [10a]	Ref. [10b]	Ref. [7]	Ref. [2]
L_3M_1 (ℓ)	ℓ'	$(3d)^1$	3.8(3)	—			—	—
$L_3M_{4,5}$ ($\alpha_{1,2}$)	α'	$(3d)^1$	3.4(1)	3.6	4.0	3.3	3.2	3.2
	α'''	$(3d)^1(4\ell)^1$	6.9(5)	5.4	5.7	5.4	4.4	4.46
	α''	$(3d)^2$	8.1(3)	8.0	8.4	8.5	7.5	7.56
L_2M_1 (η)	η'	$(3d)^1$	5(1)	—			—	—
L_2M_4 (β_1)	β_1'	$(3d)^1$	1.9(1)	2.6	4.0	2.5	2.1	2.28
	β_1'''/β_1''	$(3d)^1(4\ell)^1$	4.8(4)	3.8/5.2	5.7	3.5/5.6	3.8/5.1	3.60/5.29
	β_1^{IV}	$(3d)^2$	8.1(3)	—	8.4	—	—	—

[a] HFS assessments.
[b] Experiments with ^{4}He ions.

originated from configurations with simultaneous vacancies in $2p$ and $3d$ levels, predicting emissions with energy shifts close to those observed in the present work. Independently, Burkhalter *et al.* [10] applied the Hartree-Fock-Slater approach to LM^n configurations, where n is the number of vacancies in $3p$ or $3d$ levels, and concluded that a single $3d$ vacancy produces a 4.0 eV shift, whereas two $3d$ vacancies generate an 8.4 eV shift, both with respect to $L\alpha_{1,2}$; in addition, a $3d$ spectator hole has shown to be more likely than a $3p$ additional vacancy. The present experimental results allow to associate the $L\alpha'$ decay with a single $3d$ spectator hole, and the $L\alpha''$ line to a double $3d$ secondary vacancy event, according to the usual nomenclature; complementary, the $L\alpha'''$ line can be attributed to a combined $3d$-4ℓ spectator hole decay [10]. The energy shifts obtained are in good agreement with data reported in the literature under different experimental conditions, particularly for $L\alpha'$ and $L\alpha''$: Lucasson [7] and Cauchois and Sénémaud [2] by X-ray fluorescence experiments; Blokhin *et al.* [9], under electron excitation; and Burkhalter *et al.* [10], using ^{4}He ions.

Three satellite lines were identified in the spectral region involving the $L\beta_1$ transition, and labeled as β_1', β_1''-β_1''' (unresolved doublet), and β_1^{IV}. According to Refs. [9,10], the first emission has been associated with a $(3d)^1$ configuration; each of the β_1'' and β_1''' transitions can be assigned to a combined $3d$-4ℓ scheme; whereas the β_1^{IV} emission has been interpreted as the result of a transition with two simultaneous $3d$ vacancies. Although the energy shifts do not coincide with those observed for $L\alpha_{1,2}$, their physical origin is analogous, which leads to the same explanation based on a $(3d)^n$ scheme. The β_1' line exhibits an energy shift of 1.9 eV relative to $L\beta_1$, in agreement with the values reported by Lucasson [7] (2.1 eV), Blokhin [9] (2.6 eV), and Cauchois [2] (2.28 eV). The β_1'' and β_1''' lines, centered around an energy shift of 4.8 eV, could not be resolved in the spectral fit due to their proximity. Nevertheless, the energy of this doublet is compatible with the values reported for these satellites by Blokhin [9] (3.8 eV and 5.2 eV), Burkhalter *et al.* [10] (3.5 eV and 5.6 eV), Lucasson [7] (3.8 eV and 5.1 eV) and Cauchois [2] (3.60 eV and 5.29 eV). These lines are also attributed to $(3d)^1$ configurations, possibly involving different coupling states, which would explain their close energies —only separated under specially devoted instrumental conditions. Finally, the β_1^{IV} line, with an energy shift of 8.1 eV relative to $L\beta_1$, has not been previously measured for Ge; this value is in very good agreement with the HFS theoretical prediction provided by Burkhalter *et al.* [10], within a $(3d)^2$ approach.

The $L\ell'$ and $L\eta'$ satellite lines have not been previously measured. It must be taken into account that each of these diagram lines, along with the corresponding satellite, bear a rather low contribution to the respective line group: below 5 % in the case of $L\ell$ (L_3 group) and less than 3 % for $L\eta$ (L_2 group). The origin of these satellite emissions is attributed, by analogy with other transitions of the same group, to configurations with a spectator vacancy in the $3d$ shell. As mentioned above, such an additional vacancy will modify the effective potential within the atom in the intermediate state just before the decay, thereby shifting the energy of the emitted photon toward higher values in both transitions, whose magnitudes should be very similar, differences being associated to the orbitals involved and their coupling schemes.

Table 5 Widths and relative intensities of the satellite lines observed

Main line	Satellite	Profile	Width (eV)	Rel. intensity (%)
L_3M_1 (ℓ)	ℓ'	G	12.0(5)	47(4)
$L_3M_{4,5}$ ($\alpha_{1,2}$)	α'	G	3.2(4)	13(2)
	α'''	G	5.8(8)	12(2)
	α''	G	15.1(4)	14(1)
	Total	–	–	*39(3)*
L_2M_1 (η)	η'	G	10(2)	20(6)
L_2M_4 (β_1)	β_1'	V	1.3(5)	48(16)
	β_1''' / β_1''	V	3(2)	29(17)
	β_1^{IV}	V	5.7(6)	23(7)
	Total	–	–	*100(20)*

Table 5 summarizes the widths and relative intensities determined for the Ge satellite lines observed. These relative intensities are given as ratios to the corresponding diagram line within each transition group, corrected for differential absorption across the L_3 edge (when applicable) and for the detection efficiency. In the $L\alpha$ region, the satellite lines exhibit a rather homogeneous intensity distribution: α' with 13 %, α'' with 12 % and α''' with 14 %. Overall, the $L\alpha$ satellite lines account for 39 % of the main line intensity, a value very similar to that reported by Blokhin *et al.* [9], using electron excitation, namely, 38 %, and quite different from the 25% determined by Leiro [16].

The case of $L\beta_1$ is particularly noteworthy: the associated satellite lines reach an intensity comparable to that of the diagram line. This value is considerably high for an L2M-type transition and has not been reported in previous works under similar conditions. This unusually large ratio reflects the influence of the cross-edge differential absorption phenomenon, which is properly

accounted for in the model described in §3. In this situation, the diagram Lβ1 emission lies close to the L_3 absorption threshold, so that photons on the low-energy side of the line fall below the edge and are transmitted with higher efficiency, whereas those on the high-energy side experience an attenuation similar to that of the satellite emissions[28]. This differential behaviour enhances the relative intensity on the low-energy side, producing the observed asymmetry of the peak profile. As a result, neglecting this effect in the modelling would lead to an underestimation of the satellite-to-main intensity ratio.

The ℓ' and η' lines exhibit intensities as high as 47 % and 20 %, respectively. The determined natural widths (12.0 eV and 10 eV, respectively) are larger than the typical values for other L satellites and also exceed those of their main lines (3.9 eV for Lℓ and 4.6 eV for Lη). This suggests that these structures may represent an average of multiple nearby transitions.

Conclusions

The detailed analysis of the Ge L X-ray spectrum, carried out through a robust spectral processing method, has enabled the determination of characteristic energies, natural widths, and relative radiative transition probabilities for the main diagram lines and their associated satellite structures. The energies obtained show a good overall agreement with widely used reference data, with uncertainties below 0.2 eV for most diagram lines, validating the calibration procedure and the model used for the spectral description. Regarding the RTPs obtained, it is worth noting that they are in good agreement with Dirac-Hartree-Fock emission rates provided by Scofield, whilst they strongly disagree with EADL database.

A comprehensive identification of satellite lines was achieved for the L$\alpha_{1,2}$ and Lβ_1 transitions, including the first experimental characterization of the Ge β_1^{IV} line. Their energy shifts are in close agreement with the experimental and theoretical data available in the literature, supporting their classification within a $(3d)^n$ configuration scheme.

Encouraged by the consistency achieved by the satellite emissions associated with the main diagram transitions, the study of additional satellite features in the Lℓ and Lη regions, not previously reported for Ge, was faced. These structures exhibit large natural widths, suggesting the contribution of multiple unresolved transitions.

The remarkably high Lβ_1 satellite-to-main intensity ratio obtained here appears to be reasonable, as it arises from the careful treatment of the cross-edge differential absorption within the peak profile when the emission energy crosses the neighbouring L_3 absorption edge. This effect modifies the internal distribution of intensity across the line, producing the observed low-energy asymmetry and influencing the apparent contribution of satellite structures. By accurately accounting for this phenomenon, the present work provides insight into how self-absorption processes shape L-emission spectra and improves the physical interpretation of the observed features.

Together with the comprehensive determination of diagram and satellite parameters, the present results expand the available Ge L X-ray database and provide consistent experimental parameters that clarify the origin of several satellite features. Work is being done in order to thoroughly understand all the relaxation mechanisms involved in the occurrence of satellite emissions.

Author contributions

All authors contributed equally to conceptualization, methodology, data curation, formal analysis, validation, visualization, and writing (original draft as well as writing) review and editing. Investigation (experimental measurements) was performed by Alejo Carreras. All authors approved the final version of the manuscript.

Conflicts of interest

There are no conflicts to declare.

Data availability

All data supporting the findings of this study are available within the article.

Acknowledgements

This work was financially supported by the Secretaría de Ciencia y Técnica of the Universidad Nacional de Córdoba (UNC, Argentina), and also through a PIP2021 grant no. 11220200100986CO (CONICET, Argentina). The authors are also grateful to the Laboratorio de Microscopía Electrónica y Microanálisis (LABMEM-UNSL) where the measurements were performed.

Notes and references

1 J. A. Bearden, *Rev. Mod. Phys*, 1967, **39**, 78.
2 Y. Cauchois and C. Sénémaud, *Wavelengths of x-ray emission lines and absorption edges*, Pergamon Press, Oxford, 1978, vol. 18.
3 R. D. Deslattes, E. G. Kessler Jr., P. Indelicato, L. de Billy, E. Lindroth and J. Anton, *Rev. Mod. Phys.*, 2003, **75**, 35–99.
4 J. H. Scofield, *Phys. Rev. A*, 1974, **10**, 1507.
5 S. T. Perkins, D. E. Cullen, M. H. Chen, J. H. Hubbell, J. Rathkopf and J. H. Scofield, *Lawrence Livermore National Laboratory Report*, 1991, **UCRL-50400 30**, 1.
6 J. L. Campbell and T. Papp, *At. Data Nucl. Data Tables*, 2001, **77**, 1–56.
7 A. Lucasson, *Annales de Physique*, 1960, **13**, 509–566.
8 E. Gwinner, *Zeitschrift für Physik*, 1938, **108**, 523–541.
9 M. A. Blokhin, G. Zommer, V. F. Volkov and L. M. Monastyrskii, *Fizika Tverdogo Tela*, 1968, **11**, 17–23.
10 P. G. Burkhalter, A. R. Knudson and D. J. Nagel, *Phys. Rev. A*, 1973, **7**, 1936–1943.
11 M. Kavčič, *Phys. Rev. A*, 2003, **68**, 022713.
12 E. N. Sgourou, A. Daskalopulu, L. H. Tsoukalas, G. Stamoulis, R. V. Vovk and A. Chroneos, *Applied Sciences*, 2022, **12**, 11993.
13 P. Priyadarshini, D. Sahoo and R. Naik, *Optical and Quantum Electronics*, 2022, **54**, 166.
14 V. Baran, Y. Cat, T. Sertel, T. Ataser, N. A. Sonmez, M. Cak-

mak and S. Ozcelik, *Journal of Electronic Materials*, 2020, **49**, 1249–1256.
15 R. D. Deslattes, *Phys. Rev.*, 1968, **172**, 625–627.
16 J. A. Leiro, *Philosophical Magazine Letters*, 1988, **57**, 189–193.
17 M. Guerra, J. M. Sampaio, T. I. Madeira, F. Parente, P. Indelicato, J. P. Marques, J. P. Santos, J. Hoszowska, J.-C. Dousse, L. Loperetti, F. Zeeshan, M. Müller, R. Unterumsberger and B. Beckhoff, *Phys. Rev. A*, 2015, **92**, 022507.
18 T. Rodríguez, A. Sepúlveda, A. Carreras, G. Castellano and J. Trincavelli, *J. Anal. At. Spectrom.*, 2016, **31**, 780–789.
19 J. Goldstein, D. Newbury, D. Joy, C. Lyman, P. Echlin, E. Lifshin, L. Sawyer and J. Michael, *Scanning electron microscopy and x-ray microanalysis*, Kluwer Academic/Plenum Publishers, New York, 3rd edn., 2003.
20 J. Trincavelli, S. Limandri, A. Carreras and R. Bonetto, *Microsc. Microanal.*, 2008, **14**, 306.
21 R. Bonetto, G. Castellano and J. Trincavelli, *X-Ray Spectrom.*, 2001, **30**, 313–319.
22 S. Limandri, J. Trincavelli, R. Bonetto and A. Carreras, *Phys. Rev. A*, 2008, **78**, 022518 1–10.
23 S. Limandri, A. Carreras, R. Bonetto and J. Trincavelli, *Phys. Rev. A*, 2010, **81**, 012504 1–10.
24 K. F. J. Heinrich, Proceedings of the 11th International Congress on X-Ray Optics and Microanalysis, London, Ontario, 1987, pp. 67–119.
25 R. H. Packwood and J. D. Brown, *X-Ray Spectrometry*, 1981, **10**, 138–146.
26 J. A. Riveros and G. Castellano, *X-Ray Spectrometry*, 1993, **22**, 3–10.
27 S. J. B. Reed, *British Journal of Applied Physics*, 1965, **16**, 913.
28 A. Sepúlveda, T. Rodríguez, P. D. Pérez, A. P. L. Bertol, A. C. Carreras, J. Trincavelli, M. A. Z. Vasconcellos, R. Hinrichs and G. Castellano, *J. Anal. At. Spectrom.*, 2017, **32**, 385–392.
29 R. D. Bonetto, A. C. Carreras, J. C. Trincavelli and G. E. Castellano, *J. Phys. B*, 2004, **37**, 1477.
30 J. Campbell, *Atomic Data and Nuclear Data Tables*, 2003, **85**, 291–315.